5-28-92
E 6291

NASA Technical Memorandum 105266

Structural Analysis of Low-Speed Composite Propfan Blades for the LRCSW Wind Tunnel Model

Michael A. Ernst
Lewis Research Center
Cleveland, Ohio

January 1992

NASA

STRUCTURAL ANALYSIS OF LOW SPEED COMPOSITE PROPFAN BLADES FOR THE LRCSW WIND TUNNEL MODEL

Michael A. Ernst
NASA Lewis Research Center
Cleveland, OH

Summary

The Naval Weapons Center at China Lake, California, is currently evaluating propulsion systems for the Long Range Conventional Standoff Weapon (LRCSW). At present, the Advanced counterrotating Propfan system is being considered. The purpose of this report is to document the methodologies used to structurally analyze the 0.55 scale CM–1 composite propfan blades for the LRCSW with COBSTRAN and MSC/NASTRAN. Significant results are also reported.

Introduction

The Naval Weapons Center at China Lake, California, is currently evaluating propulsion systems for the Long Range Conventional Standoff Weapon (LRCSW). At present, the advanced counterrotating propfan system is a leading candidate (see fig. 1). The use of propfans in the propulsion systems of flight vehicles may lead to considerable fuel efficiency gains and/or an increase in range without a degradation in performance (ref. 1). Part of the evaluation process consists of fabricating a 0.55 scale proof-of-concept test rig of the LRCSW to be tested in the 14×14 foot wind tunnel at NASA Ames Research Center. NASA Lewis Research Center is presently responsible for coordinating the design, structural analysis, and fabrication of the composite propfan blades to be used in the test. To be more specific, two sets of forward and aft blades were fabricated: a low-speed set (designated the CM–1 series) and a high-speed set (designated the CM–2 series). This report documents only the methodologies used to structurally analyze the LRCSW CM–1 composite propfan blades (see fig. 2) and summarizes significant results.

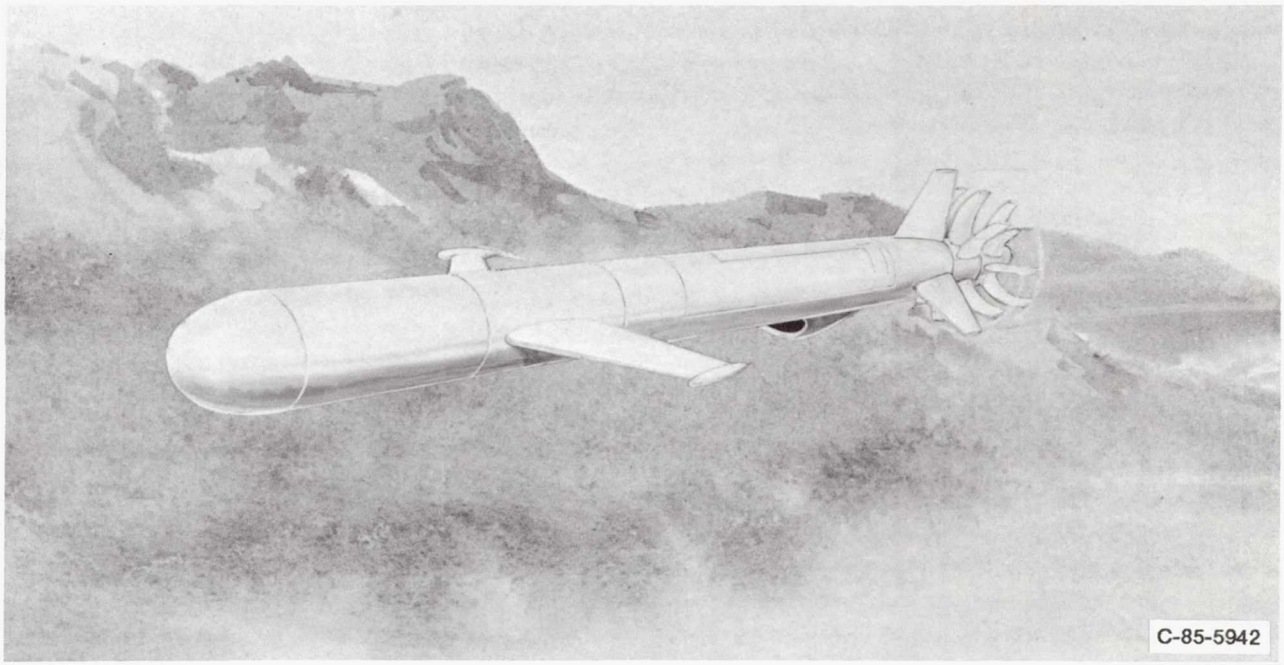

Figure 1.—Long range conventional standoff weapon.

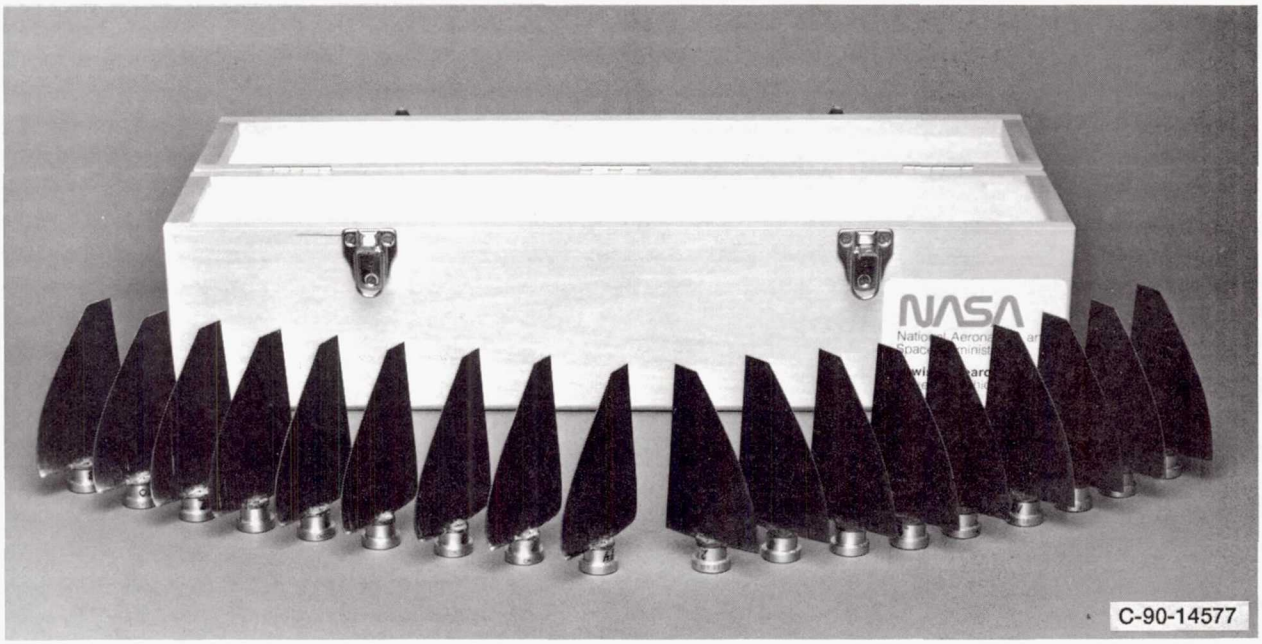

Figure 2.—CM-1D composite propfan blades.

Approach

The aerodynamic design of the LRCSW propfan blades is described in a proposed NASA technical report by C.J. MIller. The advanced counterrotating propfan system on the LRCSW test rig has 12 blades: 6 blades on the forward hub, and 6 blades on the aft hub. The hub and tip diameters for both forward and aft CM–1 blades are 8.25 and 16.5 in., respectively. The CM–1 blades were designed for a rotational speed of 9723 rpm, or a tip speed of 700 ft/sec. Overall, the counterrotating propfan system will produce a thrust of 140 lb. Initial blade designs were generated with a counterrotation strip theory code based on the work of Davidson (ref. 2). The boundary layer resulting from the long cylindrical body of the LRCSW rig was accounted for in the design. Section geometry along spanwise stations of the blades is based on an NACA 16-series airfoil, modified with additional leading- and trailing-edge thickness. This added thickness is required to accommodate four 0.0025-in. graphite fiber plies at the leading and trailing edges. Three-dimensional computational fluid dynamic meshes were generated from the blade section geometries for use in a Navier-Stokes code.

The Navier-Stokes code uses an average passage formulation to model one blade passage and is based on the Euler code reported in references 3 to 4. Blade setting angles required to match the propfan design conditions were determined from the Navier-Stokes solutions through iteration. Once the design conditions were attained, individual blade geometries and surface pressures were saved for use in the structural design process.

Figure 3 displays the methodology used to structurally design and analyze the LRCSW propfan blades. Propfan blade cross-sectional geometries and twist distributions developed in the aerodynamic design process were fed into the computer aided design (CADAM) system for the generation of three-dimensional surface models (see ref. 6). Using the three-dimensional surface geometry defined on the CADAM design system, a finite element model of each propfan blade was generated with the COBSTRAN (Composite Blade Structural Analyzer) preprocessor code (ref. 7). A nonlinear displacement analysis, with subsequent eigenvalue analysis, was conducted on each propfan blade at various rotational speeds with MSC/NASTRAN (ref. 8). Campbell diagrams produced from the analytical results were used to determine whether the blades were clear of significant engine order excitations within the design operating envelope. If not, the blade was redesigned.

Results from the MSC/NASTRAN analyses were also used to determine whether the propfan blades are aeroelastically stable. All aeroelastic analyses pertaining to the LRCSW propfan blades are described in a proposed NASA report by J.M. Lucerno. The analyses were conducted with the ASTROP2 (Aeroelastic Stability and Response of Propulsion Systems) code (ref. 11), which applies modal methodologies to determine the aeroelastic stability of propfan blades. Blade geometry, mode shapes, and frequencies generated by the above mentioned NASTRAN analyses serve as input. If any of the blades were found unstable, the blade in question was redesigned.

When the blades were found to be aeroelastically stable and when the Campbell diagrams were deemed ac-

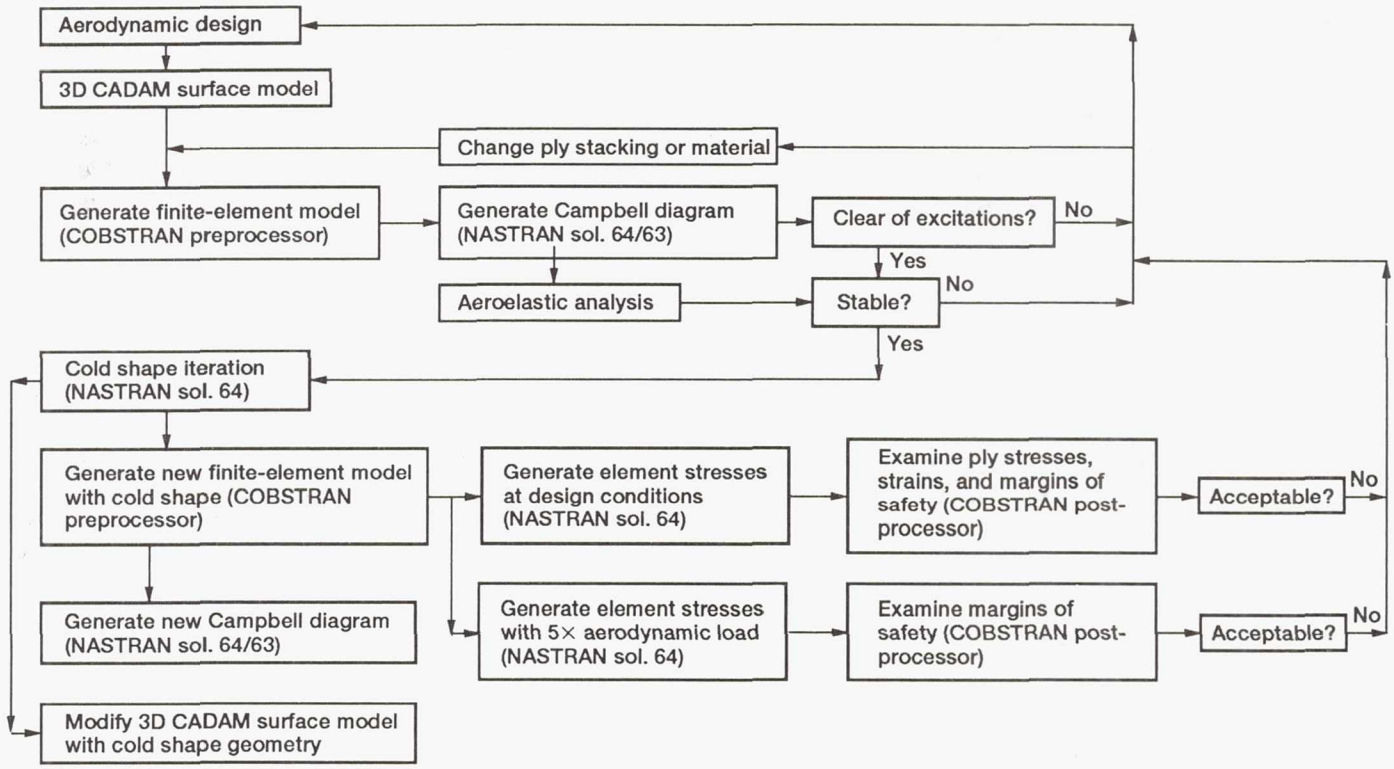

Figure 3.—Flow-chart displaying methodology used in propfan blade structural design and analysis.

ceptable, the aerodynamic and structural design of the propfan blades was frozen. Using MSC/NASTRAN's nonlinear analysis capability, the cold shape of each propfan blade was determined. "Cold shape" refers to the geometry of the propfan blade before any aerodynamic or centrifugal loads are applied. A detailed discussion of the cold shape iteration process follows in the report. With the cold shape geometry, a new finite-element model was generated for each blade with COBSTRAN's preprocessor, and the three-dimensional CADAM surface models were modified.

Next, a nonlinear displacement analysis was conducted on the new finite-element model of each respective propfan blade: centrifugal loads due to the design rotational speed and appropriate steady-state aerodynamic loads were applied. Results from these analyses were post-processed with COBSTRAN. Individual ply stresses, strains, and margins of safety were examined. If the margin of safety for any of the propfan blades falls below 1, the blade in question was redesigned.

Because of the lack of time available and the lack of proper unsteady aerodynamic forces associated with the forced excitations, unsteady stress analyses were not conducted on the propfan blades. Assuming that the amplitude of the unsteady aerodynamic forces would not be greater than a factor of 4 times its steady counterpart, the margins of safety for all propfan blades were regenerated with the air loads multiplied by five. It was reasoned that if the margins of safety were acceptable for such unreasonable air loads, the blades will withstand the unsteady loading associated with forced excitations. Again, the analyses were conducted with MSC/NASTRAN, and the results post-processed with COBSTRAN. Finally, new Campbell diagrams were generated with the cold shape geometries.

NASTRAN

MSC/NASTRAN version 65C was used for all finite-element analyses performed in this study. A version of this code exists on the NASA Lewis Research Center's Cray X-MP computer. Specifically, MSC/NASTRAN's solution sequence 3 was used for eigenvalue analyses of static propfan blades; MSC/NASTRAN's solution sequence 64 was used for nonlinear displacement analyses of rotating propfan blades; and a combined solution sequence 64/63 was used for eigenvalue analyses of rotating propfan blades.

Typical MSC/NASTRAN cards employed to run a solution 3 and 64 on a propfan finite-element model are seen in appendices A and B, respectively. Further information concerning the cards used are found in reference 8.

Typical MSC/NASTRAN cards used to run a combined solution 64/63 are shown in appendix C. The use of many of the cards listed in the executive control deck is not obvious. In the past, obtaining analytical frequencies and eigenvectors of a propfan blade experiencing high rotational speeds consisted of two steps. First, a nonlinear displacement analysis would be made on the blade in ques-

tion using MSC/NASTRAN's solution sequence 64, and both the global mass and stiffness matrices would be stored in a data base. Second, an eigenvalue analysis would be made on the blade with MSC/NASTRAN's solution sequence 63, incorporating both the global mass and stiffness matrices mentioned above. However, there is a component in the vector of centrifugal forces, dependent upon displacements associated with the translational degrees of freedom lying in the plane of rotation, that is not accounted for in the eigenvalue analysis. Because of its dependence upon the above mentioned displacements, it essentially acts as a set of softening terms in the global stiffness matrix. By not accounting for these softening terms, an essential part of the physics of the problem is missing in the MSC/NASTRAN solution 63 analysis. To remedy the problem, DMAP cards in the executive control deck, with DMI cards located in the bulk data deck, were written to add the appropriate centrifugal softening terms into the global stiffness matrix that consequently gets used by the eigenvalue analysis. Taking it one step further, the cards were written so that the solution 64 nonlinear displacement analysis and the solution 63 eigenvalue analysis could be submitted in one step. A much more detailed discussion on the use of MSC/NASTRAN in the analysis of rotating propfan blades may be found in reference 10.

COBSTRAN

All MSC/NASTRAN finite-element models pertaining to the LRCSW propfan blades were generated with the COBSTRAN (see ref. 7) code currently operating on the Cray X-MP computer at NASA Lewis. COBSTRAN consists of a preprocessor and a postprocessor (see ref. 11). Given the blade geometry and material selection, the preprocessor combines composite micromechanics and classical laminate theory with a data base of fiber and matrix properties to

```
TITLE=CM1D FORWARD MATERIAL PROPERTY GENERATION, NO SPAR
TITLE=CM1DHOT, TIP RAD. =  8.250, M = .7, RPM = 9723.000
PREPROCESSOR
SOLID BLADE
ECHO
PROPERTY INPUT
MSC NASTRAN
PLYORDER
PRTOUT
ENDOPTION
   5   3
  85  24
   1  20  14   2
  20  20  20  20  20  20  20  20  20  20  20  20  20  20  20  20  20  20  20  20
  20  20  20  20
  4.125   8.25
  4.1250 -1.1793 -0.6222 -0.6845
  4.1250 -1.0544 -0.4984 -0.6482
  4.1250 -0.9294 -0.3984 -0.5956
```

Propfan geometry

```
  8.2499  1.1305  0.7822  0.7697
0.        102.      0.       102.      0.        102.
T300 SPOX 0.003     0.02     0.6       0.
0.        102.      0.       102.      0.        102.
T300 SPOX 0.003     0.02     0.6       45.0
0.        102.      0.       102.      0.        102.
T300 SPOX 0.003     0.02     0.6       -45.0
  60
   1   1   2   1   1   3   1   1   2   1   1   3   1   1   2   1   1   3   1   1
   2   1   1   3   1   1   2   1   1   3   1   1   2   1   1   3   1   1   2   1
   1   3   1   1   2   1   1   3   1   1   2   1   1   3   1   1   2   1   1   3
   3
   1        .600E 00  .578E-01  .200E 08  .160E 07  .700E 06  .300E 00
  .200E 06  .200E 06  .770E 04  .770E 04  .130E 05
   2        .600E 00  .578E-01  .200E 08  .160E 07  .700E 06  .300E 00
  .200E 06  .200E 06  .770E 04  .770E 04  .130E 05
   3        .600E 00  .578E-01  .200E 08  .160E 07  .700E 06  .300E 00
  .200E 06  .200E 06  .770E 04  .770E 04  .130E 05
```

Figure 4.—Typical COBSTRAN preprocessor input deck.

generate a finite-element model with anisotropic homogeneous material properties. With stress output provided by NASTRAN, and with many of the data bases created during generation of the respective finite-element model, the COBSTRAN postprocessor provides individual ply stresses and strains, interply stresses, through-the-thickness stresses, and failure margins.

A typical COBSTRAN preprocessor input deck, used to generate NASTRAN finite-element models of the LRCSW propfan blades, may be found in figure 4. It must be mentioned at this point that COBSTRAN operates in a cartesian coordinate system (see fig. 5), where the X-axis is in the spanwise direction of the blade (positive from base to tip) and the Y-axis lies on the axis of rotation (positive from leading edge to trailing edge).

Referring to figure 4, the first 10 cards define the title of the problem and the various options used. Specifically, the options require COBSTRAN to generate an MSC/NASTRAN finite-element model of a solid blade where the ply order and ply material properties are to be specified by the user in the preprocessor input deck. This option forces COBSTRAN to match the user ply data input by adjusting database fiber and matrix values. User input and extended data are to be echoed in the output.

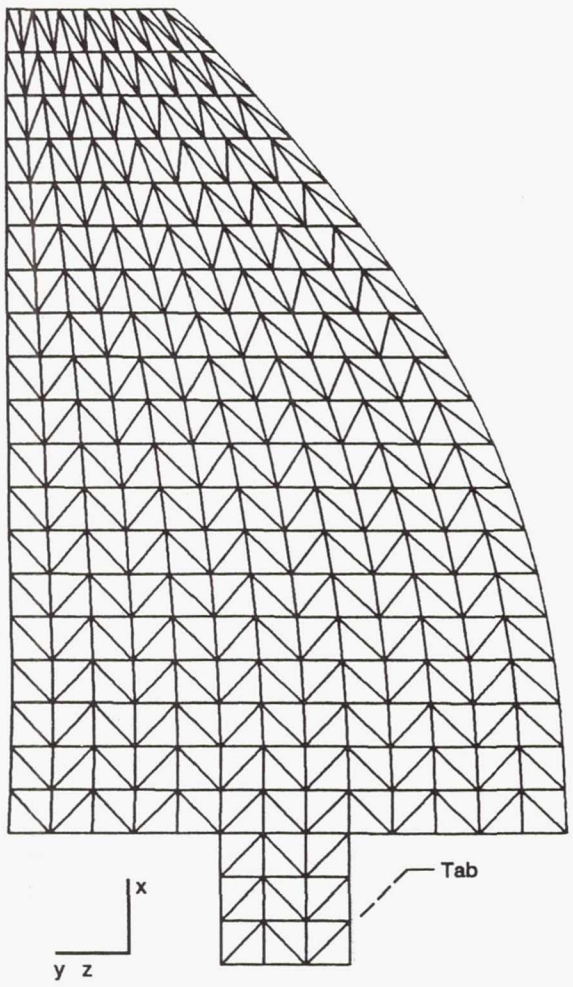

Figure 5.—A COBSTRAN-generated finite-element model of a propfan blade.

The next six cards in the input deck pertain to the blade geometry provided to COBSTRAN by the user, and to the finite-element model that COBSTRAN generates. Card 11 specifies that the material properties and the stacking order of three composite plies are to be provided by the user in the input deck and that MAT2 cards (see ref. 8) are to be generated for each element with anisotropic material properties, based on reduced axial stiffness and reduced bending stiffness. Card 12 specifies that the ply properties at node 85 of the finite-element model are to be provided in the COBSTRAN output, and the geometry of the propfan's airfoil is to be defined along 24 spanwise stations. Card 13 specifies that the finite-element model will comprise 14 equally incremented nodal points along the Y-axis for each of 20 equally incremented spanwise stations along the X-axis. The finite-element model is then to be made up of triangular elements with diagonal sides alternating across the blade. Cards 14 and 15 specify the number of geometric points used to define the blade's airfoil geometry for each spanwise station referenced on card 12. Card 16 specifies, in inches, the initial and final spanwise stations for the finite-element model's mesh.

Although not shown in figure 4, the next 480 cards refer to the geometry of the propfan blade in question. Starting with the propfan's base leading edge and working to the tip trailing edge, each card simultaneously defines an upper surface and a lower surface nodal point. Columns 1 to 4 refer to the X, Y, Z upper surface, and Z lower surface coordinate positions, respectively.

The last 17 cards of the input deck pertain to the composite plies that COBSTRAN uses when structurally modeling the blade. Following the geometric input are three groups of two cards. Each group refers to a different composite ply. All three composite plies are alike except for the ply orientation angles: ply 1 is oriented at 0° from the X-axis; ply 2 is oriented at 45° from the X-axis; and ply 3 is oriented at -45° from the X-axis. All three plies are 0.003 in. thick, have a void volume ratio of 0.02, and have a fiber volume ratio of 0.6.

The next four cards pertain to the stacking sequence of the composite plies. First, the number of plies is specified for the half-thickness at the point where maximum blade thickness occurs. Normally, this is a number that is equal to, or greater than, half the total number of plies used by the respective propfan blade. For LRCSW propfan blades, the number 60 is used. This is a number that is greater than half the total number of plies used in the fabrication of these blades. Second, the stacking sequence is specified starting with the outside ply. Finally, the last six cards pertain to the composite material properties of plies

TABLE I.—COMPOSITE MATERIAL PROPERTIES USED IN DESIGN AND COLD SHAPE ITERATION

[Ply thickness, 0.003 in.; void volume fraction, 0.02; fiber volume ratio, 0.6.]

(a) Material properties

Fiber volume ratio	0.600
Weight density, lb/in.^{3}	0.578×10^{-01}
Longitudinal modulus, lb/in.^{2}	0.200×10^{08}
Transverse modulus, lb/in.^{2}	0.160×10^{07}
Shear modulus, lb/in.^{2}	0.700×10^{06}
Poisson's ratio	0.300

(b) Ply strengths

Longitudinal tensile strength, lb/in.^{2}	0.200×10^{06}
Longitudinal compressive strength, lb/in.^{2}	0.200×10^{06}
Transverse tensile strength, lb/in.^{2}	0.770×10^{04}
Transverse compressive strength, lb/in.^{2}	0.770×10^{04}
Intralaminar shear strength, lb/in.^{2}	0.130×10^{05}

```
TITLE = CM1D FORWARD BLADE
TITLE = PLOADS INCLUDED
POSTPROCESSOR
SOLID
PRTOUT
MSC NASTRAN
ENDOPTION
```

Figure 6.—Typical COBSTRAN postprocessor input deck.

1 to 3. Table I summarizes the composite material properties used.

A typical COBSTRAN postprocessor input deck, used for all LRCSW propfan blades, is shown in figure 6. Unlike the preprocessor input deck, only option cards are required here. Specifically, COBSTRAN is to postprocess an MSC/NASTRAN finite-element model of a solid composite propfan blade.

Modeling of Shank

Up to this point, the approach used to generate an MSC/NASTRAN finite-element model of an LRCSW propfan blade has been discussed. However, there is still the matter of generating the respective shank associated with the blade model being analyzed. The shanks associated with each LRCSW propfan blade consist of three components: a stainless-steel shell; a composite tab (see fig. 5) within the shell; and filler material between the composite tab and the shell. Both the stainless-steel shell and the shank filler material are modeled with simple beam elements seen in appendix D. The Young's modulus and the shear modulus for the metal shank shell are 2.85×10^7 and 1.12×10^7 psi, respectively; while the Young's modulus, shear modulus and Poisson's ratio for the filler material are 2.15×10^7 psi, 7.0×10^5 psi, and 0.469, respectively.

The approach taken to model the composite tab of the respective propfan shank consists of three steps. First, a new finite-element model is generated whose cross-sectional profile is equal to that of the blade's base and whose spanwise coordinates begin at the base of the shank shell and end at the base of the respective propfan blade. Second, elements and grid cards are removed such that only a tab equal in width to the shank shell is left. Third, identification numbers for all the MSC/NASTRAN bulk data deck cards are altered, such that the tab model is compatible with the finite-element model of the propfan blade.

Again, referring to figure 4, let's assume one is given a set of COBSTRAN formatted nodal points that define the geometry of a particular LRCSW propfan blade. Again, each card simultaneously defines an upper and lower surface nodal point, starting at the base leading edge of the blade, and working its way to the trailing edge tip. The first number of cards, n, defining the geometry of the blade's base are retained, while the remainder of the cards are removed. The number n corresponds to the first number shown on card 14 of figure 4. The cards that remain are duplicated at a spanwise station of 3.461 in., which happens to coincide with the base of the shank. Now, $2\times n$ cards exist and are inserted into the COBSTRAN input deck where normally the nodal points defining the geometry of a particular propfan blade would go.

Various cards in the input deck need to be altered to account for the shank model being generated. Specifically, the node number on card 12, whose ply properties are listed in the output, needs to be altered. Also, now only two spanwise stations exist that define the new model in COBSTRAN; therefore, the number 24 needs to be changed to 2. The value on card 13 that specifies the number of equally incremented spanwise stations along the X-axis needs to be changed to 4 (the value that specifies the number of equally incremented nodal points along the Y-axis of the finite-element model must remain the same so that the final tab model is compatible with the respective blade model). Cards 14 and 15 need to be modified to account for the fact that only two sets of COBSTRAN nodal geometry points exist that define the new model, rather than 24. And finally, the new model starts at a spanwise station of 3.461 in. and ends at a spanwise station of 4.125 in.; therefore, card 16 needs to be altered. All remaining cards of the input deck remain unchanged.

The finite-element model generated by COBSTRAN may be seen in figure 7. The cross-sectional geometry is exactly the same as the central region of the base of the propfan finite-element model shown in figure 5. Elements 11 to 16, 37 to 42, and 63 to 68 are retained, while all other elements are discarded. Now a composite tab exists that is geometrically compatible with the shank shell and the base of the respective propfan blade. The shank model

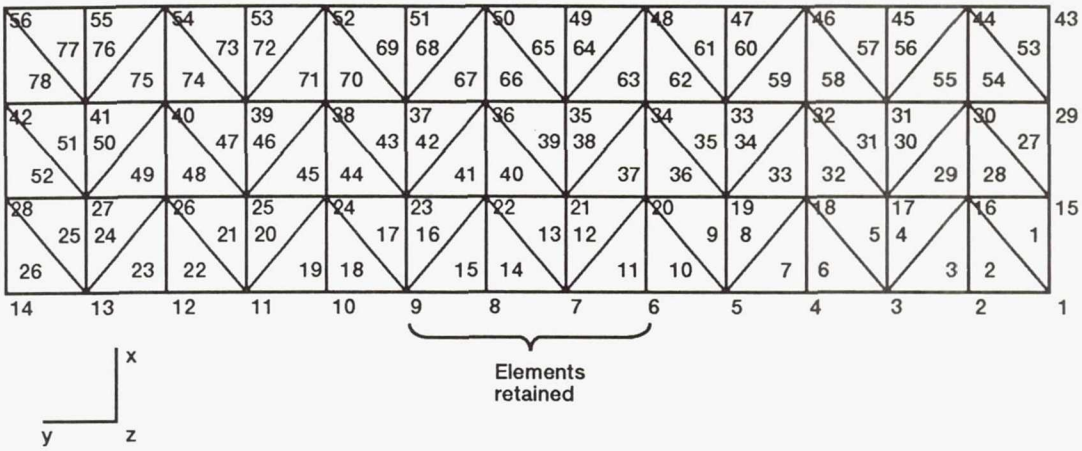

Figure 7.—Work plot for generation of tab finite-element model.

is finally complete (as shown in fig. 8) by changing the identification numbers on all the remaining NASTRAN bulk data deck cards that may conflict with those in the existing propfan finite-element model.

Cold Shape Iteration

The propfan geometry that results from the aerodynamic design process is generally labeled the "hot shape."

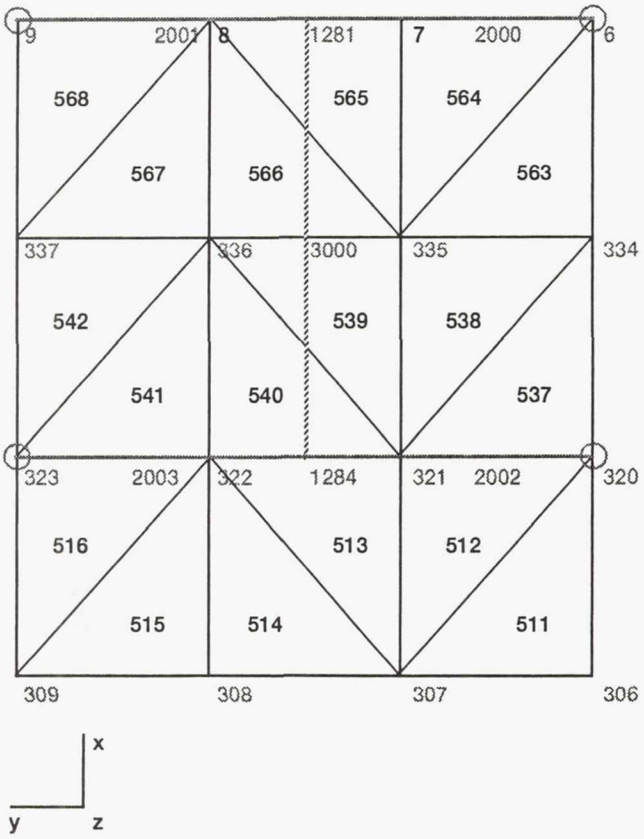

Figure 8.—Typical finite element model of blade shank.

"Hot shape" refers to the geometry of the propfan blade that is desired after it has experienced aerodynamic and centrifugal loading. Much of the preliminary analyses discussed in the subsequent sections of this paper are based on the hot-shape geometry of the respective propfan blades. After many design iterations, a particular hot shape needs to be selected and a cold shape determined.

In the first step, a NASTRAN solution 64 nonlinear displacement analysis is made on the hot shape geometry of a particular propfan blade. Aerodynamic and centrifugal loads associated with the respective design point are included, displacing the original hot shape geometry. The displacements that result from the analysis are subtracted from the hot shape geometry, which leads to a preliminary cold shape geometry. To maintain the logistics of the problem, let's call this new geometry cold shape 1. The second step consists of running a nonlinear displacement analysis on cold shape 1. Again, aerodynamic and centrifugal loads are included. The displacements that result from the analysis are added to cold shape 1, and a comparison is made with the desired hot shape. If the maximum difference between the hot shape and cold shape with added displacements is larger than 0.001 in., all the differences are subtracted from cold shape 1 (which will be labeled cold shape 2) and step 2 is repeated with the new cold shape. Step 2 continues to be repeated until the maximum difference between the hot shape and cold shape with added displacements is less than 0.001 in. at all locations on the airfoil.

A case analogous to what was described above is shown with the 1 degree of freedom problem of figure 9. A mass, M, is attached to a nonlinear spring, K. The hot shape for this particular model (fig. 9(a)) is such that the mass is a distance a from the fixed end of the spring. A steady force, F (fig. 9(b)), is applied to the mass, and the resulting displacement is d_1. Figure 9(c) represents the cold shape after the first iteration, where the mass is a distance of $(a - d_1)$ from the fixed end. Applying load F on the cold shape model (fig. 9(d)), a new displacement arises

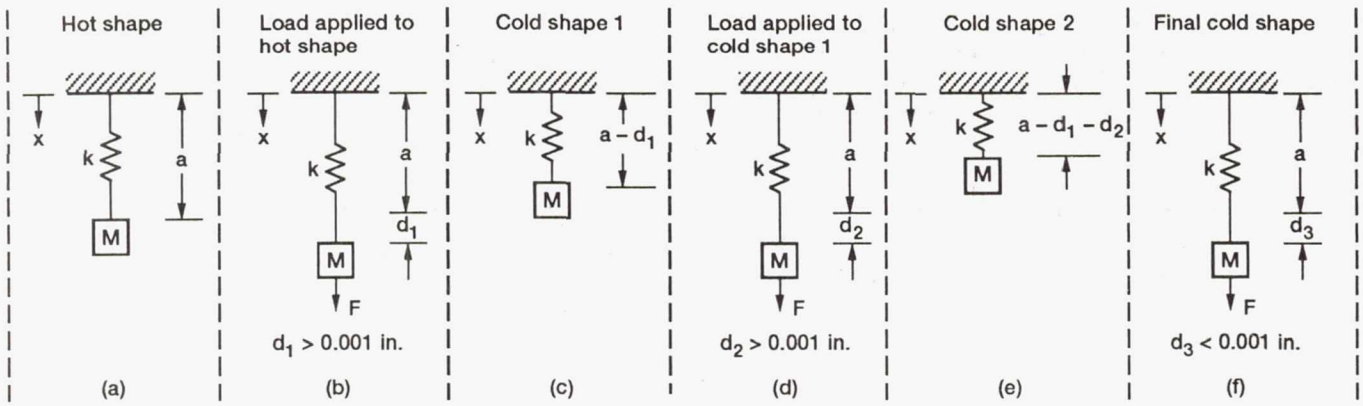

Figure 9.—Schematic of cold shape interation.

such that the difference between the original hot shape and the cold shape with added displacement is equal to d_2. The difference is not yet less than 0.001 in.; thus, another iteration takes place, where the new cold shape is represented in figure 9(e). Here, the distance of the mass from the fixed end of the spring is $(a - d_1 - d_2)$. After applying the load one last time (fig. 9(f)), the difference between the hot shape and the new cold shape with added displacement is equal to d_3, which happens to be less than 0.001 in. Thus, the final cold shape has been found, and is equal to $(a - d_1 - d_2)$.

Analytical Results for CM–1

The purpose of this section of the paper is to present the results obtained from the structural analyses conducted on CM–1 blade designs. In particular, this section presents Campbell diagrams for the CM–1A, CM–1B, CM–1C, and CM–1D forward and aft blades; CM–1D stress results; CM–1D geometric changes due to the cold shape iteration; CM–1D margins of safety; and CM–1D mass and center of gravity correlations with the respective computer-aided design (CAD) model. CM–1 versions A to D refer to design iterations. Design details associated with CM–1 versions A to D are found in reference 6.

All CM–1 propfan blades are designed for a rotational velocity of 9723 rpm, or for a tip speed of 700 ft/sec. The CM–1D stress analyses, whose results are presented later, were conducted at this design point.

All MSC/NASTRAN finite-element models used in the CM–1 propfan analyses consist of 280 nodal points and 494 triangular elements. Specifically, the models comprise of

14 equally incremented nodal points along the axis of rotation and 20 equally incremented nodal points along the spanwise axis. The CM–1 blades have a span of 4.125 in., where the base of the blade is located at the 4.125 in. radial station and the tip of the blade is located at the 8.25 in. radial station.

Table I presents the composite ply material properties used by COBSTRAN to generate the finite-element models associated with the iterative design process and the cold shape iteration. The composite plies have a thickness of 0.003 in., with a void volume ratio of 0.02 and a fiber volume ratio of 0.6.

Table II presents the composite ply material properties used by COBSTRAN to generate finite-element models associated with all analyses conducted after the cold-shape iteration. These material properties were supplied by the material vendor. The composite plies were 0.0032 in. thick; the void volume ratio and fiber volume ratio remain unchanged. Because of the insignificant change in material properties, the cold shape iteration process was not repeated.

Starting with the outside ply and working through to the point of mid thickness, the plies are stacked at 0°, 0°, 45°, 0°, 0°, -45°, ..., with respect to the spanwise axis. Finally, applying the right-hand-rule, all forward blades rotate about the *Y*-axis, while the aft blades rotate in the

TABLE II.—COMPOSITE MATERIAL PROPERTIES USED AFTER COLD-SHAPE ITERATION

[Ply thickness, 0.0032 in.; void volume fraction, 0.02; fiber volume ratio, 0.6.]

(a) Material properties

Fiber volume ratio	0.604
Weight density, lb/in.^{3}	0.560×10^{-01}
Longitudinal modulus, lb/in.^{2}	0.194×10^{08}
Transverse modulus, lb/in.^{2}	0.120×10^{07}
Shear modulus, lb/in.^{2}	0.700×10^{06}
Poisson's ratio	0.310

(b) Ply strengths

Longitudinal tensile strength, lb/in.^{2}	0.266×10^{06}
Longitudinal compressive strength, lb/in.^{2}	0.266×10^{06}
Transverse tensile strength, lb/in.^{2}	0.930×10^{04}
Transverse compressive strength, lb/in.^{2}	0.930×10^{04}
Intralaminar shear strength, lb/in.^{2}	0.130×10^{05}

opposite direction. Blade setting angles are measured with respect to the plane of rotation.

Campbell Diagrams During Design Iteration

The generation of the CM–1 Campbell diagrams consists of running nonlinear displacement and subsequent eigenvalue analyses on each of the forward and aft blades at the respective rotational speeds associated with blade tip velocities of 450, 600, and 750 ft/sec. A simple eigenvalue analysis is also conducted to determine the modal frequencies of the blades without centrifugal loading. Results for the first six modal frequencies are tabulated, and the frequencies (in hertz) are plotted against the respective rotational speed (in rpm). Because of a lack of empirical data, no preset margins are imposed on the operating conditions on the Campbell diagram.

Four engine order excitations are of concern in the structural design of the CM–1 forward and aft blades and are therefore included on the Campbell diagrams. Specifically, forced excitations due to LRCSW angle of attack, wakes generated by upstream LRCSW wings and fins, and aerodynamic interaction between the forward and aft sets of blades are represented on the Campbell diagrams by 1-, 2-, 4-, and 12-per-revolution excitation lines, respectively.

Campbell diagrams for the CM–1A forward and aft blades may be found in figure 10. The blade setting angle for the forward blade, measured from the 75-percent radial station, is 59.90°; the aft blade has a setting angle of 57.61°. Tabulated data may be found in table III. As shown, the second and third modes of both the forward and aft blades are experiencing 12-per-revolution excitations within the operating envelope of the LRCSW test rig.

With a 15-percent increase in outboard camber over that of the CM–1A blades, the CM–1B forward and aft blades offered very little in terms of alleviating the problem mentioned above. Figure 11 presents the Campbell diagrams for the CM–1B forward and aft blades, respectively. Again, the second and third modes are experiencing 12-per-revolution excitations within the operating envelope. (See table IV for the tabulated data.) The blade setting angle for the forward blade, measured from the 75 percent radial station, is 58.48°; the aft blade has a setting angle of 56.38°.

Campbell diagrams for the CM–1C forward and aft blades are shown in figure 12. The setting angles for these blades have not changed from those of the CM–1B blades. The CM–1C blades have a 10 percent increase in midspan thickness over that of the CM–1A blades. As seen, the third mode is clear of any excitation within the operating envelope, and the eigenvalues associated with the second mode increased (table V).

Campbell diagrams for the CM–1D forward and aft blades are shown in figure 13. The blade setting angle for

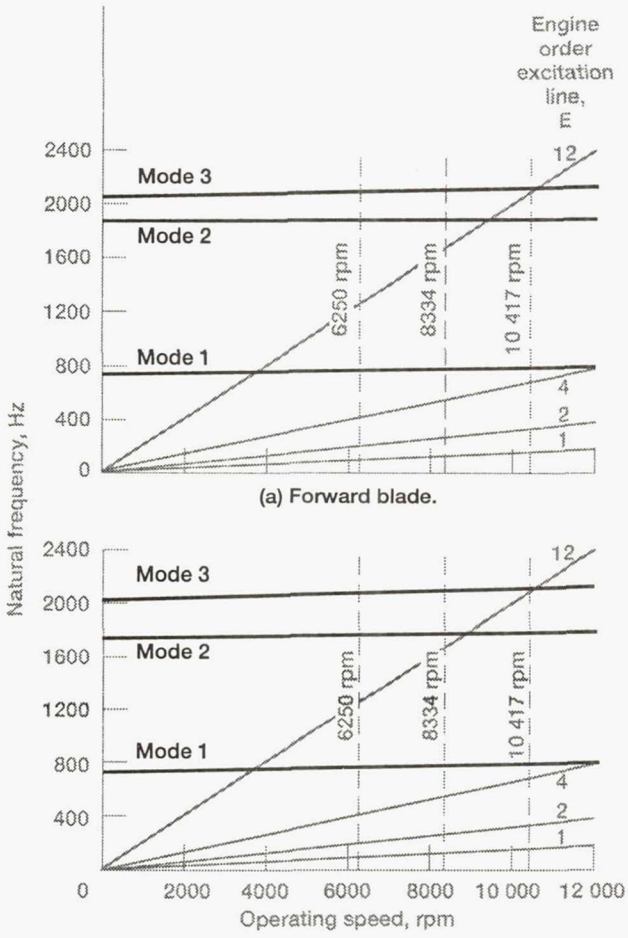

Figure 10.—CM-1A Campbell diagrams.

TABLE III.—MODAL FREQUENCIES FOR CM-1A BLADES

(a) Forward blade

Eigenvector	Propfan tip speed, ft/sec			
	0	450	600	750
	Modal frequency, Hz			
1	750.0	772.4	789.2	809.9
2	1871.4	1880.0	1886.1	1893.6
3	2046.8	2071.5	2090.8	2115.4
4	2866.1	2873.8	2879.7	2887.3
5	3240.4	3245.0	3248.6	3253.1
6	3669.7	3688.8	3702.9	3720.2

(b) Aft blade

1	739.7	762.9	780.2	801.5
2	1761.0	1773.0	1782.0	1792.8
3	2031.6	2060.7	2083.2	2111.3
4	2795.4	2808.2	2818.0	2830.1
5	3231.2	3236.8	3241.0	3246.4
6	3643.7	3668.3	3687.1	3709.8

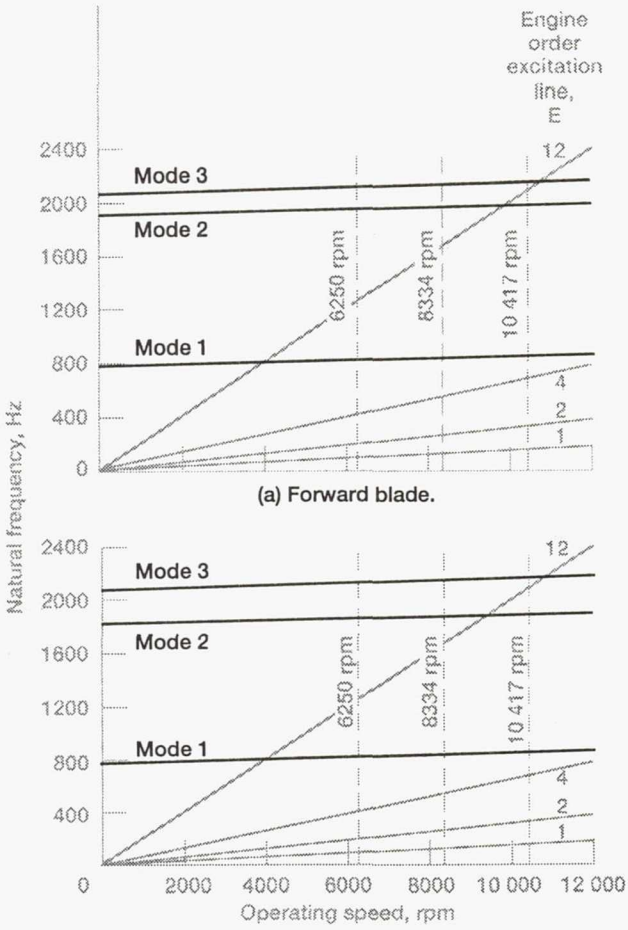

(a) Forward blade.

(b) Aft blade.

Figure 11.—CM-1B Campbell diagrams.

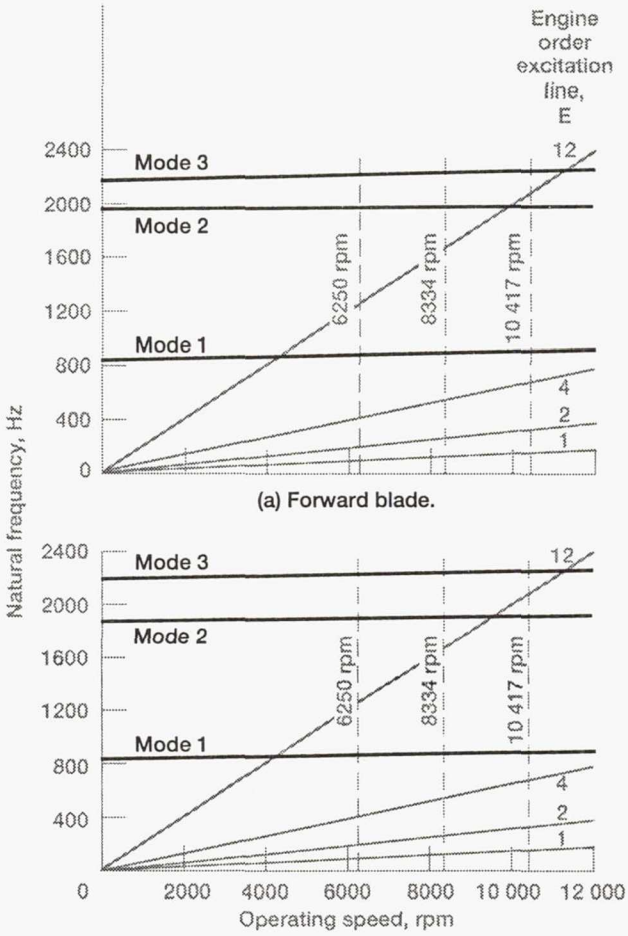

(a) Forward blade.

(b) Aft blade.

Figure 12.—CM-1C Campbell diagrams.

TABLE IV.—MODAL FREQUENCIES FOR CM-1B BLADES

(a) Forward blade

Eigen-vector	Propfan tip speed, ft/sec			
	0	450	600	750
	Modal frequency, Hz			
1	797.5	819.9	836.6	857.3
2	1922.4	1940.3	1952.7	1967.0
3	2082.2	2099.1	2113.2	2132.4
4	2913.4	2920.6	2926.1	2933.1
5	3391.9	3399.8	3405.6	3412.6
6	3680.3	3702.0	3718.4	3738.8

(b) Aft blade

1	782.0	806.1	824.0	846.0
2	1829.0	1849.6	1864.4	1881.8
3	2086.0	2107.7	2125.5	2148.5
4	2882.8	2895.5	2905.4	2917.5
5	3483.3	3491.2	3496.8	3503.3
6	3628.6	3655.6	3678.1	3706.0

TABLE V.–MODAL FREQUENCIES FOR CM-1C BLADES

(a) Forward blade

Eigen-vector	Propfan tip speed, ft/sec			
	0	450	600	750
	Modal frequency, Hz			
1	848.2	867.0	881.1	898.1
2	1961.0	1971.7	1979.4	1988.7
3	2148.8	2205.1	2221.0	2241.7
4	2962.7	2970.5	2976.4	2984.0
5	3103.2	3108.0	3111.7	3116.4
6	3903.1	3921.6	3935.3	3952.2

(b) Aft blade

1	834.3	854.0	868.9	887.2
2	1883.7	1898.7	1909.6	1922.8
3	2200.9	2222.8	2239.8	2261.5
4	2935.1	2946.8	2955.6	2966.5
5	3166.5	3172.1	3176.4	3181.9
6	3878.8	3902.7	3920.3	3941.9

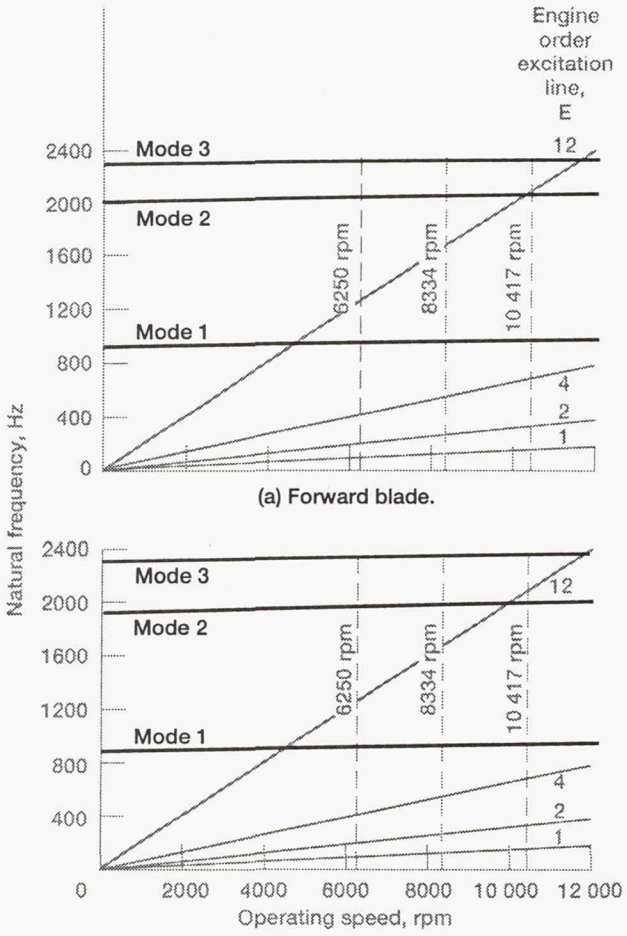

Figure 13.—CM-1D Campbell diagrams.

the forward blade, measured from the 75 percent radial station, is 64.49°; the aft blade has a setting angle of 58.90°. The CM–1D blades have a 10-percent increase in midspan thickness over the CM–1B blades. Like the CM–1C blades, the third mode is clear of any excitations. The second mode of both the forward and aft blades still experiences a 12-per-revolution excitation; however, the frequencies associated with this mode are higher than that of the CM–1C blades. (See table VI.) Because of project time constraints, the CM–1 forward and aft blade designs are frozen at design iteration D.

CM–1D Cold Shape Analyses

The nonlinear displacement analysis associated with the cold shape iteration process was conducted at the design rotational speed of 9723 rpm. Respective steady-state air loads were included in the analyses. Two iterations were required to find the cold shape of both the forward and aft CM–1D blades.

The cold shape and hot shape twist distributions are given in table VII for the CM–1D forward and aft blades.

TABLE VI.—MODAL FREQUENCIES FOR CM-1D BLADES

(a) Forward blade

Eigenvector	Propfan tip speed, ft/sec			
	0	450	600	750
	Modal frequency, Hz			
1	911.9	929.8	943.4	960.3
2	2006.2	2024.4	2037.8	2054.1
3	2291.7	2302.8	2311.8	2324.0
4	3034.4	3040.0	3044.2	3049.7
5	3323.3	3328.2	3331.9	3336.7
6	3903.1	3923.5	3938.9	3957.9
(b) Aft blade				
1	892.0	911.7	926.5	944.8
2	1928.4	1948.5	1963.2	1981.1
3	2300.3	2316.9	2330.0	2346.9
4	2981.3	2992.2	3000.5	3010.8
5	3386.2	3391.3	3395.3	3400.3
6	3872.9	3899.7	3919.5	3943.8

TABLE VII.— TWIST DISTRIBUTION OF CM-1D BLADES

(b) Forward blade

Radial station, percent span	Cold shape	Hot shape
	Twist distribution, deg	
50.0	60.78	60.74
52.6	66.93	66.88
55.3	68.63	68.58
57.9	69.03	68.97
60.5	68.99	68.93
63.2	68.68	68.60
65.8	68.07	67.99
68.4	67.20	67.11
71.0	66.19	66.08
73.7	65.11	65.00
76.3	64.09	63.98
78.9	63.11	62.99
81.6	62.15	62.03
84.2	61.18	61.07
86.8	60.22	60.12
89.5	59.31	59.22
92.1	58.42	58.36
94.7	57.45	57.44
97.4	56.45	56.51

(b) Aft blade

Radial station, percent span	Cold shape	Hot shape
	Twist distribution, deg	
50.0	67.12	67.10
52.6	66.26	66.23
55.3	65.36	65.33
57.9	64.51	64.47
60.5	63.62	63.58
63.2	62.75	62.70
65.8	61.87	61.81
68.4	61.05	60.97
71.0	60.22	60.14
73.7	59.41	59.31
76.3	58.60	58.48
78.9	57.81	57.68
81.6	57.08	56.92
84.2	56.31	56.13
86.8	55.57	55.37
89.5	54.88	54.66
92.1	54.20	53.97
94.7	53.48	53.26
97.4	52.90	52.69

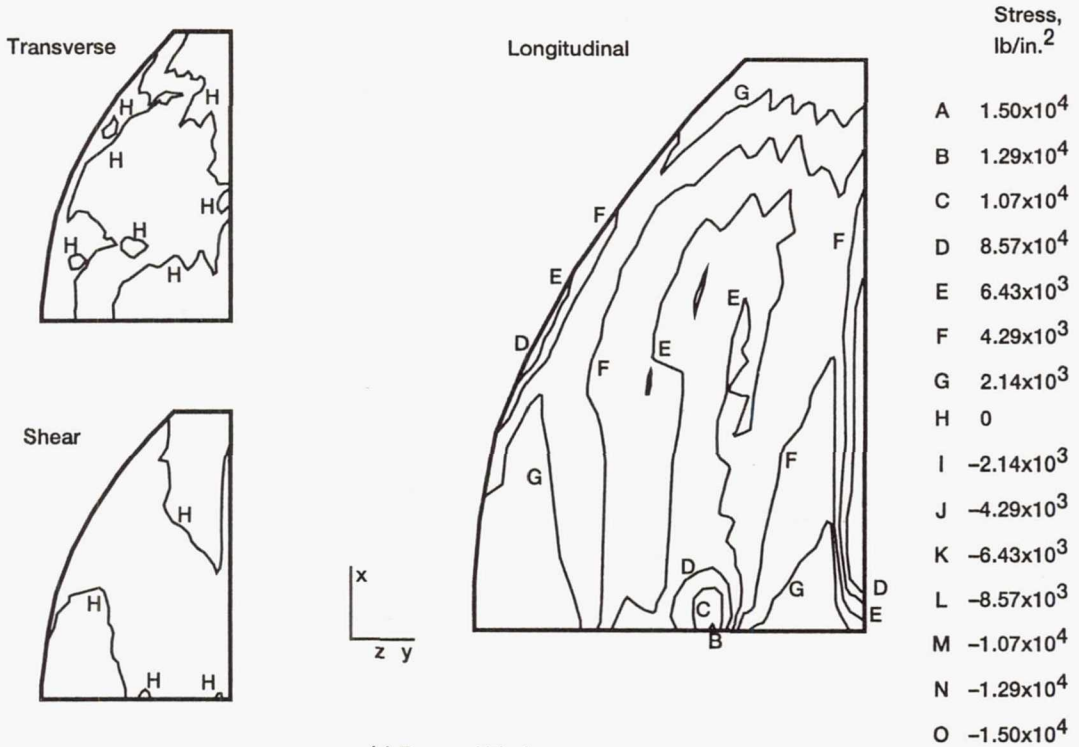

(a) Forward blade.

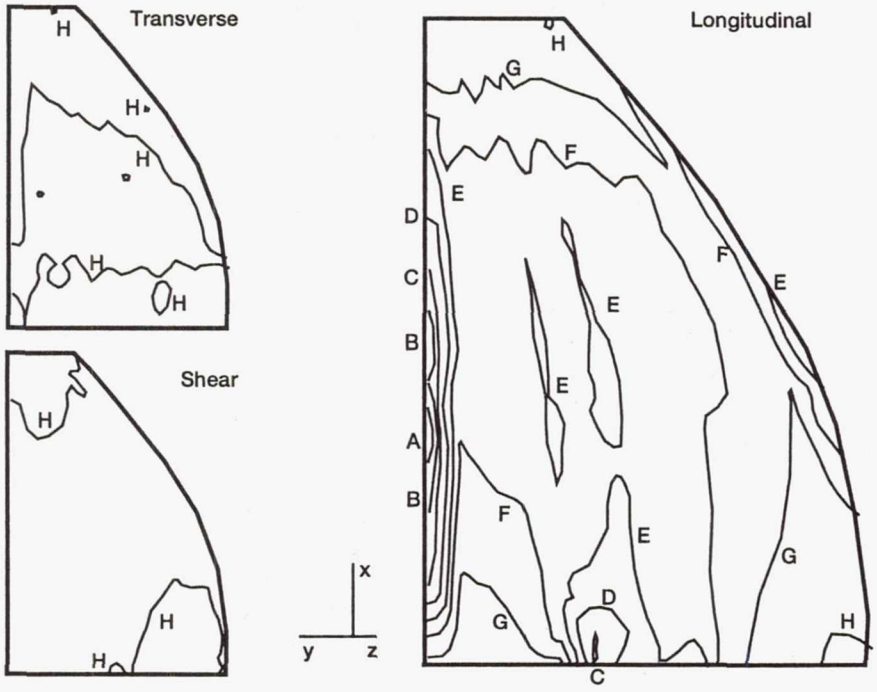

(b) Aft blade.

Figure 14.—CM-1D stress plots; pressure side.

At the 3/4 radial blade station, the blade setting angle decreases by a 0.1° for both blades. Total displacement at the tip leading edge of the CM–1D forward blade is 0.035 in. Total displacement at the tip leading edge of the CM–1D aft blade is 0.033 in. Overall, the results of the cold shape iteration process indicate that the CM–1D forward and aft blades are very stiff when analyzed under the design conditions.

Figure 14 presents the surface stresses associated with the pressure side of the forward and aft CM–1D blades. Figure 15 presents the surface stresses associated with the suction side of the forward and aft CM–1D blades. In the analyses, the forward and aft blades were subjected to a centrifugal load resulting from the design rotational speed: the design rotational speed was 9723 rpm. Steady-state aerodynamic loads were applied to the respective finite-element models with MSC/NASTRAN's PLOAD2 cards (see ref. 8). Postprocessing of MSC/NASTRAN results is conducted with COBSTRAN.

The longitudinal stresses associated with the pressure side of the forward and aft blades are primarily tensile in nature. Both blades exhibit a stress concentration where the aft end of the shank shell meets the base of the blade. High stresses also occur along the thin trailing edges of the blades. As expected, transverse and shear stresses are comparatively small.

The longitudinal stresses associated with the suction side of both forward and aft blades tend to be compressive. High compressive stresses are primarily located along the trailing edge of both blades near the base of the blades. Again, transverse and shear stresses are comparatively small.

The Campbell diagrams for the CM–1D forward and aft blades with the cold shape geometry are shown in figure 16, and the tabulated frequencies in table VIII. The blade setting angle for the forward blade, measured from the 75 percent radial station, is 64.60°; the aft blade has a setting angle of 59.00°.

Because of the comparatively small difference between the cold shape and hot shape geometries of the CM–1D blades, the Campbell diagrams offer nothing new. Again, the only concern within the operating range of the propfan blades is the possible 12-per-revolution excitation of the second mode.

Figure 17 presents the contour plots of the first six analytically predicted mode shapes associated with the CM–1D forward and aft blades at 0 rpm. The predicted fifth mode for both forward and aft blades is an axial, or edgewise, mode.

The margins of safety for both the CM–1D forward and aft blades were obtained from the output of COBSTRAN's postprocessor. Two runs were made for each blade at the design point; one with the respective steady air loads associated with the design point, and the other with the air loads multiplied by a factor of five.

Figure 18 presents the minimum margins of safety for both the CM–1D forward and aft blades. As shown, the margins of safety are well above five for both blades. Unlike the aft blade, a stress concentration can be seen on the forward blade near the shank. This is not unexpected. Low margins of safety can be seen along the extreme leading and trailing edges; however, experience has shown this is caused by numerical problems within the code rather than by the physics of the problem.

Figure 19 presents the minimum margins of safety for both forward and aft blades experiencing steady air loads multiplied by a factor of five. The margins of safety remain above zero for both blades, indicating a high degree of confidence in the structural integrity of both blades during forced excitations. Both figures are excellent representations of the stress flow due to the centrifugal forces and the extreme magnitude of the aerodynamic forces. Stress flow appears to move smoothly into the shank regions of both blades. Stress values in the tip trailing-edge regions as well as regions forward and aft of the shank, near the base of the blades, appear relatively benign.

Mass and Center of Gravity Correlation with CAD Model

The objective of this task was to correlate the mass of the CM–1D NASTRAN finite-element model with the mass of CM–1D CAD solid model. The correlation is intended to show whether the finite-element models are accounting for all structural mass of the CM–1D design. The approach taken was to make an MSC/NASTRAN solution 64 run for both the CM–1D forward and aft blades. Both mass and center-of-gravity locations were recorded from the output. Mass and center-of-gravity locations were then obtained from the CM–1D CAD solid models, and a comparison was made. If there were any significant discrepancies between the NASTRAN model and the CAD model, the cause was found and the finite-element model corrected.

Results from the above task, for both the forward and aft blades, are shown in table IX. Columns 1 and 2 list the mass and center-of-gravity locations obtained from both the finite-element and CAD models. As seen, there was a significant difference in mass between the finite-element model and CAD model of both the forward and aft blades. Specifically, there was a 0.37-in. difference in center-of-gravity locations along the span. The cause of this discrepancy was that the base of the shank shell, or the portion of the shank below the constrained model, was not accounted for in both the forward and aft finite-element models. Because the unmodeled portion of the shank lies below the constraints for both blades and because the global mass and stiffness matrices of the finite-element models are not influenced, concentrated weights of 0.0286 and 0.0285 lb were added to the base of the CM–1D forward and aft blades, respectively, to account for the un-

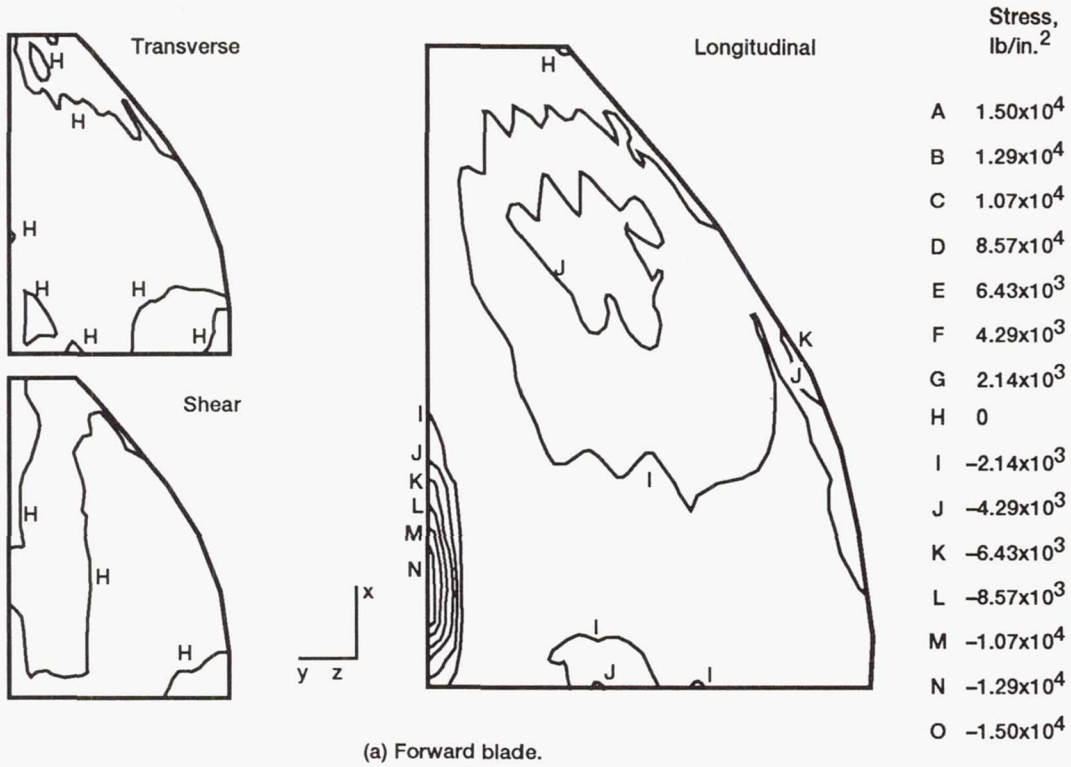

(a) Forward blade.

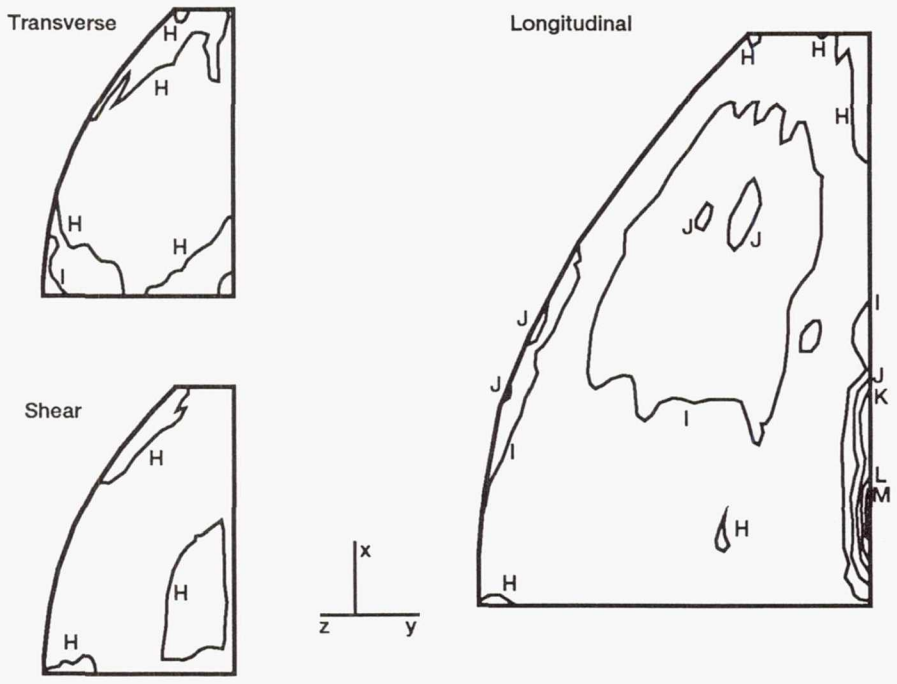

(b) Aft blade.

Figure 15.—CM-1D stress plots; suction side.

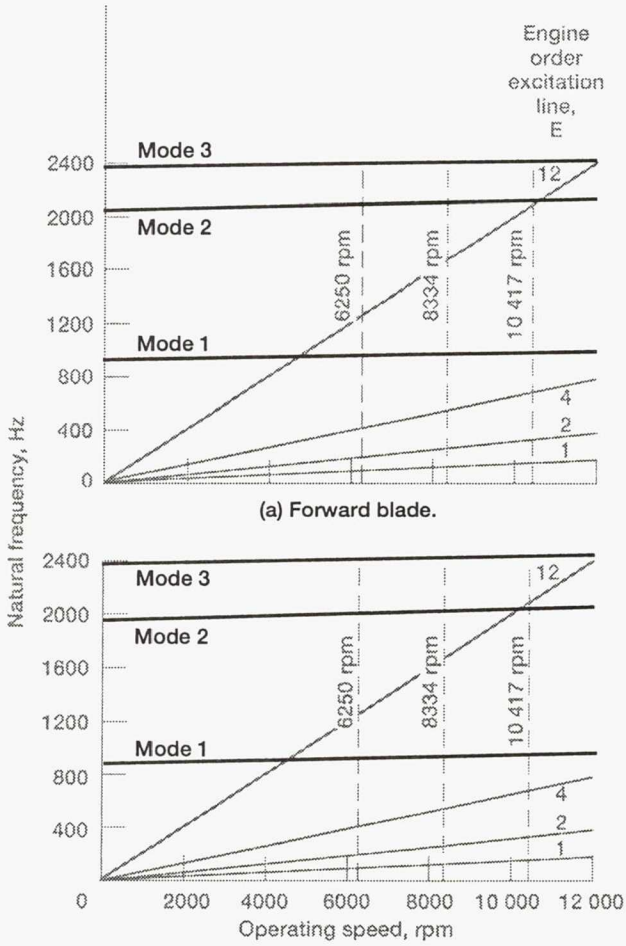

(a) Forward blade.

(b) Aft blade.

Figure 16.—CM-1DX Campbell diagrams.

TABLE VIII.—MODAL FREQUENCIES FOR CM-1D FORWARD BLADE

[Cold Shape with revised Material Properties.]

(a) Forward blade

Eigen-vector	Propfan tip speed, ft/sec			
	0	450	600	750
	Modal frequency, Hz			
1	931.9	950.2	963.9	981.0
2	2044.3	2065.1	2080.4	2098.7
3	2369.7	2379.9	2388.2	2399.6
4	3106.7	3113.0	3117.7	3123.7
5	3417.4	3422.1	3425.7	3430.2
6	3991.0	4012.3	4028.0	4046.9

(b) Aft blade

1	909.0	929.4	944.5	963.2
2	1958.2	1981.6	1998.4	2018.5
3	2365.6	2382.0	2394.9	2411.7
4	3021.1	3033.5	3042.6	3053.8
5	3483.7	3488.8	3492.6	3497.6
6	3936.4	3963.5	3983.2	4006.8

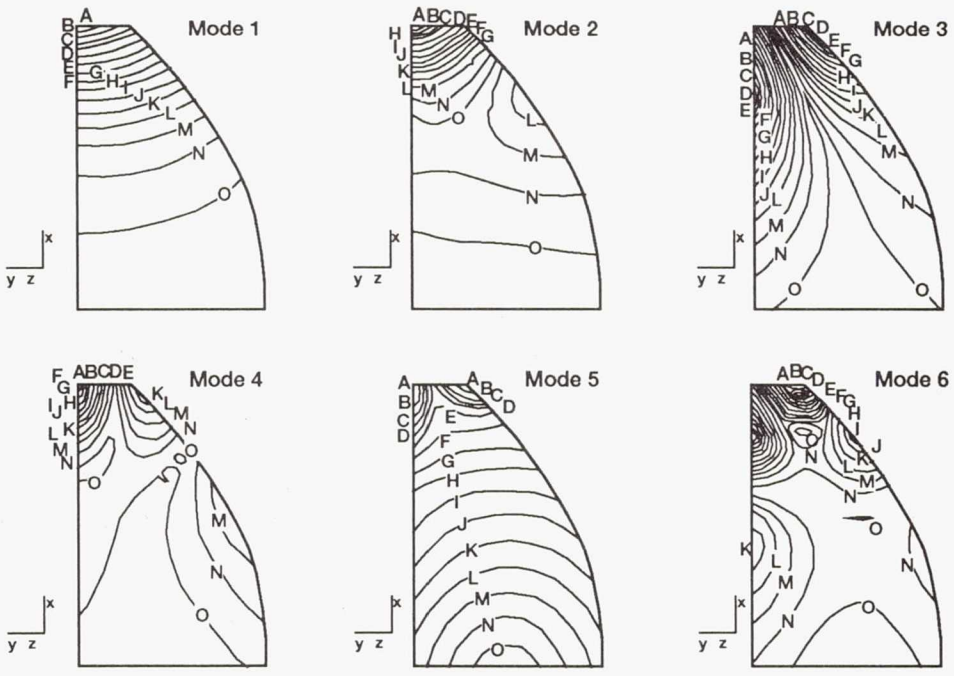

(a) Forward blade.

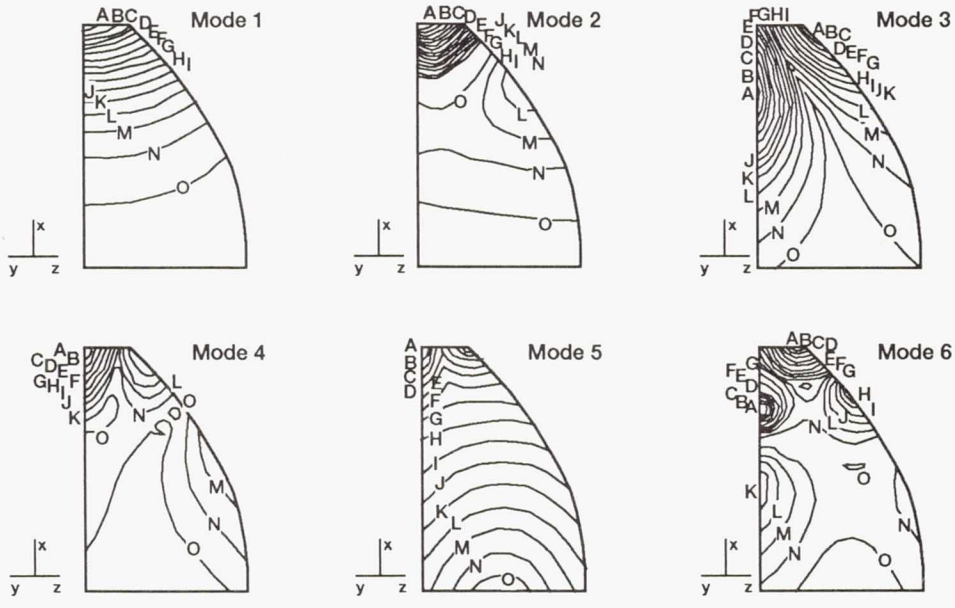

(b) Aft blade.

Figure 17.—Contour plots of modal displacement associated with the CM-1D blades.

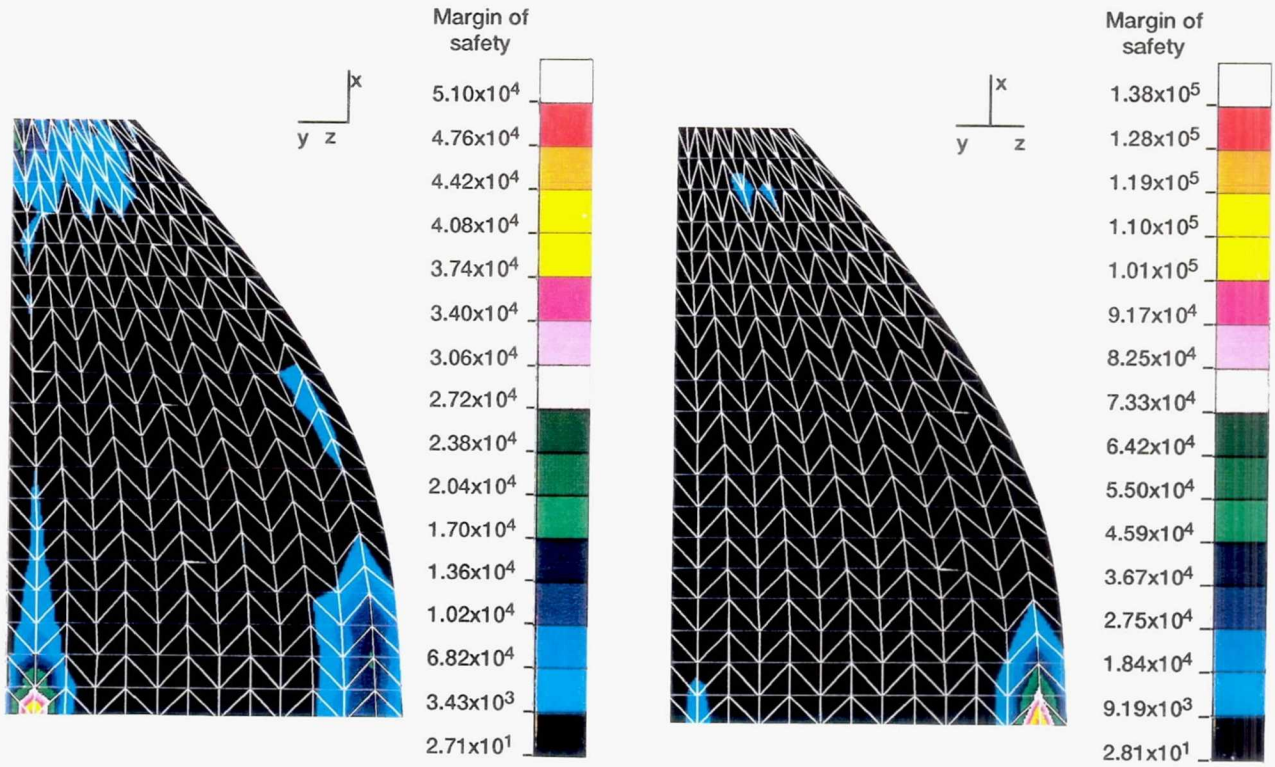

(a) Forward blade. (b) Aft blade.

Figure 18.—Minimum margins of safety for CM-1DX. Design speed with airloads.

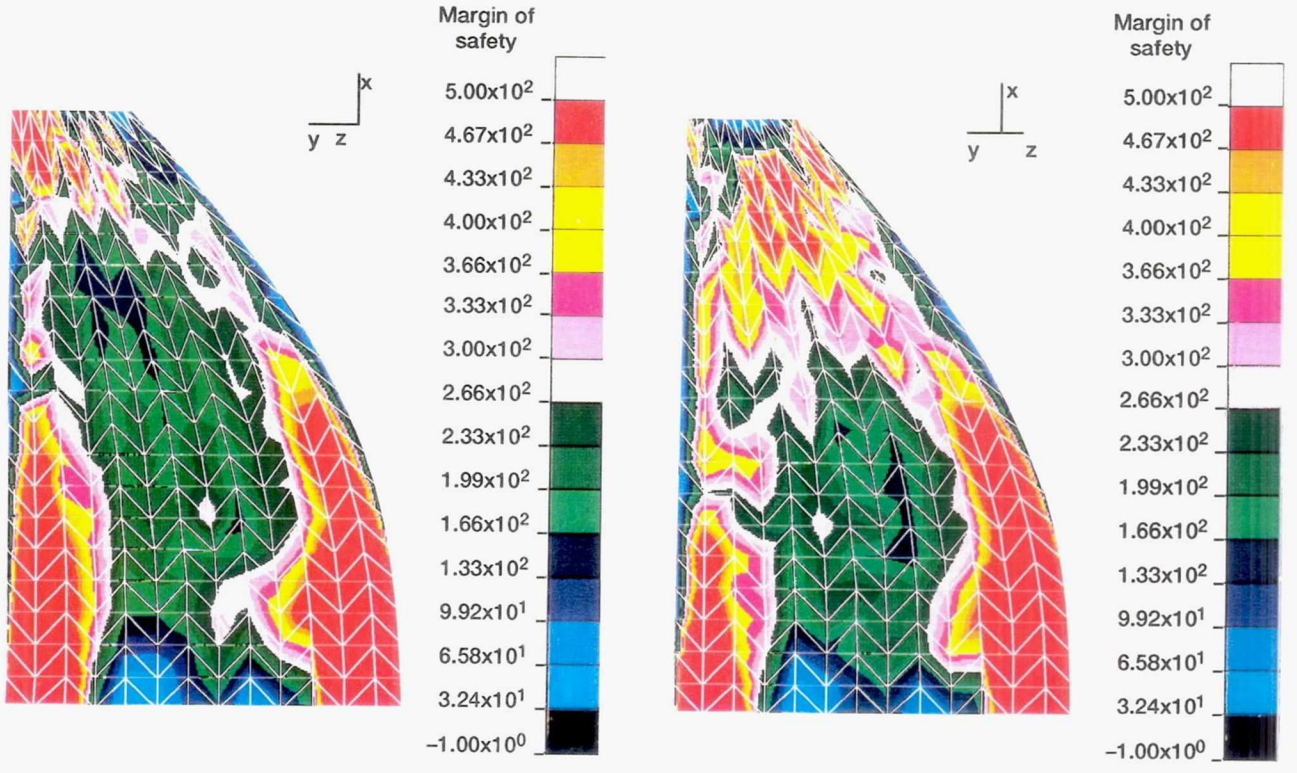

(a) Forward blade. (b) Aft blade.

Figure 19.—Minimum margins of safety for CM-1DX. Design speed with 5 times the airloads.

Page intentionally left blank

Table IX.—CM–1D Blade Mass comparison of Finite Element Model (FEM) and GADAM Model.

(a) Forward blade

	FEM	CAD	NEW FEM
Mass, lb	7.671×10^{-2}	1.043×10^{-1}	1.053×10^{-1}
Center-of-gravity location, in.; for—			
X	4.931	4.562	4.562
Y	4.999×10^{-2}	3.196×10^{2}	3.859×10^{-2}
Z	5.347×10^{-2}	3.187×10^{2}	5.036×10^{-2}

(b) Aft blade

Mass, lb	7.633×10^{-2}	1.044×10^{-1}	1.048×10^{-1}
Center-of gravity location, in.; for—			
X	4.933	4.561	4.563
Y	4.685×10^{-2}	2.893×10^{-2}	3.642×10^{-2}
Z	-5.826×10^{-2}	-3.527×10^{-2}	-5.316×10^{-2}

modeled portion of the shank. MSC/NASTRAN solution 64 runs were again made on both the forward and aft CM–1D finite-element models, and the results may be seen in columns 3 of tables IX.

Summary of Results

In summary, the CM–1D forward and aft blades were selected as the final designs for the LRCSW low-speed test. Both forward and aft blade designs are analytically experiencing 12-per-revolution integral-order excitations within the operating envelope; however, the resonance condition is avoidable without seriously impeding the goals of the wind tunnel test. At design, the margins of safety are well above five, and a high degree of confidence exists with regard to the structural integrity of the LRCSW propfan blades during forced excitations.

Appendix A
Typical MSC/NASTRAN Solution 3 Input Deck

```
ID USER, NAME
APP DISP
SOL 3
TIME 10
CEND
TITLE = CM-1 FORWARD BLADE, SOL 3, COLD SHAPE
SUBTITLE = LAYUP 0/0/-45/0/0/45....; B3/4=64.60
    SPC = 222
    DISP = ALL
    STRESS = ALL
    METHOD = 111
BEGIN BULK
$
PARAM       GRDPNT 0
PARAM       MAXRATIO2.0+15
PARAM       AUTOSPC YES
EIGR,111,SINV,0.0,5000.,,12,,,+E1
+E1,MASS
$
$$$$$$$$$$$$$$$$$$$$$$$$ BLADE FINITE ELEMENT MODEL
$
   -
   -
   -
   -
   -
ENDDATA
```

Appendix B
Typical MSC/NASTRAN Solution 64 Input Deck

```
ID USER, NAME
APP DISP
SOL 64
TIME 10
CEND
TITLE = CM-1D FORWARD BLADE, SOL 64, COLD SHAPE, RPM = 9723,
SUBTITLE = LAYUP 0/0/-45/0/0/45....; B3/4=64.60
        SET 1 = 1 THRU 494
        SET 2 = 1 THRU 280
        SPC = 222
        LOAD = 100
SUBCASE 1
        LABEL = LINEAR STATIC
SUBCASE 2
        LABEL = DIFFERENTIAL STIFFNESS
        PARAM,NOMECH,1
SUBCASE 3
        LABEL = SUBCASE 3
SUBCASE 4
        LABEL = SUBCASE 4
SUBCASE 5
        LABEL = SUBCASE 5
SUBCASE 6
        LABEL = SUBCASE 6
SUBCASE 7
        LABEL = SUBCASE 7
SUBCASE 8
        LABEL =SUBCASE 8
SUBCASE 9
        LABEL = SUBCASE 9
SUBCASE 10
        LABEL = SUBCASE 10
SUBCASE 11
        LABEL = SUBCASE 11
SUBCASE 12
        LABEL = SUBCASE 12
SUBCASE 13
        LABEL = SUBCASE 13
SUBCASE 14
        LABEL = SUBCASE 14
        DISP(PRINT,PUNCH) = 2
        PARAM,NOMECH,-1
        SPCFORCE = ALL
BEGIN BULK
$
PARAM           GRDPNT          0
PARAM           MAXRATIO2.0+15
PARAM           AUTOSPC         YES
RFORCE 100      0               162.05      0.0         1.0         0.0
$
$$$$$$$$$$$ BLADE FINITE ELEMENT MODEL
$
        -
        -

        -
        -
        -
ENDDATA
```

Appendix C
Typical MSC/NASTRAN Combined Solution 64/63 Input Deck

```
Executive Control Deck
ID USER1NAME
APP DISP
SOL 64
TIME 10
$ $ $ $ $ $ $ $ $ $ $ $ $ $ $ $ $ $ $ $ $ $ $ $ $ $ $ $ $ $ $ $ $ $ $ $ $ $ $ $
$
ALTER 77          $ FOR SOL 64 VERSION 63 ONLY
PARAM     //SUB/V,N,MSUBS/V,Y,NSUBS/1  $$ FOR EIGENVALUE ANALYSIS
PARAMR    //MPY/V,N,OMEGA/V,Y,RPM/.1047198 $
PARAMR    //MPY/V,N,0MEGASQ/OMEGA/OMEGA  $
PARAMR    //COMPLEX//OMEGASQ/0.0/V,N,ALPHAC $
MATMOD    K1,,,,,/K1BOB,/5/LUSET $
ADD       K1BOB,/K10M/ALPHAC
MPYAD     K10M,MJJ,/KSOFT/0/-1//1/6 $
DBSTORE   KSOFT,//MODEL/0/ $
MATMOD    K2,,,,,/K2BOB,/5/LUSET $
DBSTORE   K2BOB,//MODEL/0/ $
ALTER 188         $
DBFETCH   /HKSOFT,,,,1MODEL/0/1 $
ADD       KJJ,HKSOFT/KTOT// $
EQUIV     KTOT,KJJ/ALWAYS $
COND      NOMECH1,NOMECH $
DBFETCH   /HK2BOB,,,,/MODEL/0/1 $
PARAMR    //C,N,COMPLEX//V,Y,KFIXR/0.0/V,N,KFIXC $
ADD       HK2BOB,/KKFIX/KFIXC $
ADD       KKFIX,KJJ/KTTT// $
EQUIV     KTTT,KJJ/ALWAYS  $
LABEL     NOMECHI  $
ALTER 315   $$ INCLUDE FOR EIGENVALUE EXTRACTION SOL 64 VERSION 63
DBFETCH   /DYNAMICS,MJJ,GM,,/MODEL/0/0 $
DBFETCH   /GKAA,,,,/SOLID/0/1 $
MATMOD    MJJ,,,,,/NVEC,/12/S,N,NULLS/2 $
EQUIV     MJJ,MNX/MPCF1 $
COND      LBLB3,MPCF1 $
MCE2      GUSET,GM,MJJ,,,/MNX,,, $
LABEL     LBLB3 $
COND      LBLB1,NULLS $
SCEI      GUSET,MNX,,,/MXBOB,,,,, $
JUMP      LBLB2 $
LABEL     LBLB1 $
EQUIV     MNX,MXBOB/ALWAYS $
LABEL     LBLB2 $
DPD       DYNAMICS,GPLS,SILS,USET,SLT,/GPLD,SILD,USETD,,,,,,,EED,
          EQDYN/LUSET/V,N,LUSETD/V,N,NOTFL/V,N,NODLT/V,N,NOPSDL/
          V,N,NOFRL/V,N,NONLFT/V,N,NOTRL/V,N,NOEED/C,N,0/V,N,NOUE $
READ      GKAA,MXBOB,,,EED,GUSET,CASECC/LAMA,VECTOR,
          MI,OEIGS/MODES/S,N,NEIGS/NSUBS $
OFP       LAMA,OEIGS// $
COND      FIN,NEIG5 $
SDRI      GUSET,,VECTOR,,,,GM,,,,/UGV,,QG/I/REIG $
SDR2      CASECC,FCSTMS,FMPT,FDIT,FEQEXINS,,FETT,,FBGPDT,LAMA,QG,
          UGV,EST,XYCDB/OPG1,OQG1,0UGV1,OES1,OEF2,PUGV/REIGEN/-1 $
OFP       OUGV1,OPG1,OQG1,OEF2,OES1// $
LABEL     FIN $
```

```
PRTPARM ////1 $

ENDALTER
CEND
```

Case Control Check

```
TITLE = CM-1D FORWARD BLADE, SOL 63/64, COLD SHAPE, RPM = 9723,
SUBTITLE = LAYUP 0/0/-45/0/0/45....; B3/4=64.60
        SET 1 = 1 THRU 494
        SET 2 = 280
        SPC = 222
        LOAD = 100
        DISP = ALL
SUBCASE 1
        LABEL = LINEAR STATIC
SUBCASE 2
        LABEL = DIFFERENTIAL STIFFNESS
        PARAM,NOMECH,1
SUBCASE 3
        LABEL = SUBCASE 3
SUBCASE 4
        LABEL = SUBCASE 4
SUBCASE 5
        LABEL = SUBCASE 5
SUBCASE 6
        LABEL = SUBCASE 6
SUBCASE 7
        LABEL = SUBCASE 7
SUBCASE 8
        LABEL =SUBCASE 8
SUBCASE 9
        LABEL = SUBCASE 9
SUBCASE 10
        LABEL = SUBCASE 10
SUBCASE 11
        LABEL = SUBCASE 11
SUBCASE 12
        LABEL = SUBCASE 12
SUBCASE 13
        LABEL = SUBCASE 13
SUBCASE 14
        LABEL = SUBCASE 14
        STRESS(PRINT,PUNCH) = 1
        PARAM,NOMECH,-1
SUBCASE 15
        LABEL = EIGEN PROBLEM
        DISP = ALL
        METHOD = 111
```

Bulk Data Deck

```
BEGIN BULK
PARAM,NSUBS,15
PARAM,KFIXR,1.0
```

```
PARAM,KDIAG,0.0
PARAM  GRDPNT 0
PARAM  MAXRATIO2.0+15
PARAM  AUTOSPC YES
PARAM,RPM,9723. $RPM
RF0RCE 100    0                  162.05    0.0       1.0       0.0
DMI      K1   0         6        1         1                   6         6
DMI      K1   1         1        1.000
DMI      K1   3         3        1.000
DMI      K2   0         6        1         1                   6         6
DMI      K2   6         6        1.000
EIGR,111,SINV,0.0,5000.,,12,,,+E1
+E1,MASS
$
$$$$$$$$$$$$$$$ BLADE FINITE ELEMENT MODEL
$
          -
          -
          -
          -
          -
ENDDATA
```

Appendix D
Finite Element Model of Shank Shell and Filler Material

```
$
$$$$$$$$$$$$$$$$$$$$$$$$$ BAR ELEMENT FOR METAL SHANK SHELL
$
GRID        1281              4.12500    0.00800  0.04550
GRID        1284              3.68200    0.00800  0.04550
CBAR        1000      1000      1284       1281        6
PBAR        1000      1000   0.08891    0.00572  0.00572   0.01145
$ 17-4 PH H900
MAT1        1000    2.85+7    1.12+7
$
$$$$$$$$$$$$$$$$$$$$$$$$$ FILLER MATERIAL
$
CBEAM       3000      3000      1281       1284        6
PBEAM       3000      3000   0.11057    2.587-3   4.22-4      0.0   0.00301     0.0+PB2
+PB2          NO       1.0   0.06598    1.181-3   1.20-4      0.0   0.00130     0.0+PB3
+PB3         1.0       1.0       0.0        0.0      0.0      0.0       0.0         0.0
MAT1          3000 2.15+7    0.70+6       .4697
$
```

References

1. Strack, W.C.; et al.: Technology and Benefits of Aircraft Counter Rotation Propellers. NASA TM-82983, 1981.
2. Davidson, R.E.: Optimization and Performance Calculation of Dual-Rotation Propellers. NASA TP 1948, 1981.
3. Celestina, M.L.; Mulac, R.A.; and Adamczyk, J.J.: A Numerical Simulation of the Inviscid Flow through a Counter-Rotating Propeller. NASA TM–87200, June 8–12, 1986.
4. Adamczyk, J.J.; Mulac, R.A.; and Celestina, M.L.: A Model for Closing the Inviscid Form of the Average-Passage Equation System. NASA TM–87199, June 8–12, 1986.
5. Adamczyk, J.J.; Celestina, M.L.; Beach, T.A. and Barnett, M.: Simulation of Three-Dimensional Viscous Flow within a Multistage Turbine. ASME 89–GT–152.
6. Thorp, S.A.; Downey, K.M.: Computer Aided Design and Manufacturing of Composite Propfan Blades for LRCSW Wind Tunnel Model. NASA TM-105269, 1992.
7. Aiello, R.A.; Chamis, C.C.: Composite Blade Structural Analyzer (COBSTRAN) Theoretical/Programmer's Manual. NASA TM–101958, August 1989.
8. McCormick, C.W.; ed.: MSC/NASTRAN User's Manual, Vol. I, MacNeal-Schwendler, 1983.
9. Kaza, K.R.V.; et al.: Analytical Flutter Investigation of a Composite Propfan Model. NASA TM–88944, 1987.
10. Lawrence, C.; et al.: A NASTRAN Primer for the Analysis of Rotating Flexible Blades. NASA TM–89861, 1987.
11. Aiello, R.A.: Composite Blade Structural Analyzer (COBSTRAN) User's Manual. NASA TM–101461, 1989.

REPORT DOCUMENTATION PAGE

Form Approved
OMB No. 0704-0188

Public reporting burden for this collection of information is estimated to average 1 hour per response, including the time for reviewing instructions, searching existing data sources, gathering and maintaining the data needed, and completing and reviewing the collection of information. Send comments regarding this burden estimate or any other aspect of this collection of information, including suggestions for reducing this burden, to Washington Headquarters Services, Directorate for information Operations and Reports, 1215 Jefferson Davis Highway, Suite 1204, Arlington, VA 22202-4302, and to the Office of Management and Budget, Paperwork Reduction Project (0704-0188), Washington, DC 20503.

1. AGENCY USE ONLY (*Leave blank*)	2. REPORT DATE	3. REPORT TYPE AND DATES COVERED
	January 1992	Technical Memorandum

4. TITLE AND SUBTITLE
Structural Analysis of Low-Speed Composite Propfan Blades for the LRCSW Wind Tunnel Model

5. FUNDING NUMBERS
WU-535-03-0B

6. AUTHOR(S)
Michael A. Ernst

7. PERFORMING ORGANIZATION NAME(S) AND ADDRESS(ES)
National Aeronautics and Space Administration
Lewis Research Center
Cleveland, Ohio 44135-3191

8. PERFORMING ORGANIZATION REPORT NUMBER
E-6291

9. SPONSORING/MONITORING AGENCY NAMES(S) AND ADDRESS(ES)
National Aeronautics and Space Administration
Washington, D.C. 20546-0001

10. SPONSORING/MONITORING AGENCY REPORT NUMBER
NASA TM-105266

11. SUPPLEMENTARY NOTES
Responsible person, Michael A. Ernst, (216) 433-6035.

12a. DISTRIBUTION/AVAILABILITY STATEMENT
Unclassified - Unlimited
Subject Category 39

12b. DISTRIBUTION CODE

13. ABSTRACT (*Maximum 200 words*)
The Naval Weapons Center at China Lake, California, is currently in the process of evaluating propulsion systems for the Long Range Conventional Standoff Weapon (LRCSW). At present, the Advanced Counter-Rotating Propfan system is being considered. The purpose of this report is to document the methodologies used to structurally analyze the 0.55 scale CM1 composite propfan blades for the LRCSW with COBSTRAN and MSC/NASTRAN. Significant results are also reported.

14. SUBJECT TERMS	15. NUMBER OF PAGES
NASTRAN; Cruise missiles; Fan blades	28
	16. PRICE CODE: A03

17. SECURITY CLASSIFICATION OF REPORT	18. SECURITY CLASSIFICATION OF THIS PAGE	19. SECURITY CLASSIFICATION OF ABSTRACT	20. LIMITATION OF ABSTRACT
Unclassified	Unclassified	Unclassified	